Direct birefringence and transmission modulation via dynamic alignment of P3HT nanofibers in an advanced opto-fluidic component

GLEB S. LOBOV,[1,*] **ALEKSANDRS MARININS,**[1] **SEBASTIÁN ETCHEVERRY,**[2] **YICHEN ZHAO,**[1] **ELENA VASILEVA,**[1] **ABHILASH SUGUNAN,**[3] **FREDRIK LAURELL,**[4] **LARS THYLÉN,**[5,6] **LECH WOSINSKI,**[1] **MIKAEL ÖSTLING,**[1] **MUHAMMET S. TOPRAK,**[7] **AND SERGEI POPOV**[1]

[1]School of Information and Communication Technology, (KTH) Royal Institute of Technology, Stockholm 16440, Sweden
[2]Department of Fiber Optics, Acreo Swedish ICT, Stockholm 16440, Sweden
[3]Chemistry, Materials and Surfaces Unit, SP Technical Research Institute of Sweden, Stockholm 11486, Sweden
[4]School of Engineering Sciences, (KTH) Royal Institute of Technology, Stockholm 10691, Sweden
[5]Hewlett-Packard Enterprise Laboratories, Palo Alto, CA 94304, USA
[6]School of Biotechnology, (KTH) Royal Institute of Technology, Stockholm 10044, Sweden
[7]School of Science, (KTH) Royal Institute of Technology, Stockholm 10691, Sweden
*lobov@kth.se

Abstract: Poly-3-hexylthiophene (P3HT) nanofibers are semiconducting high-aspect ratio nanostructures with anisotropic absorption and birefringence properties found at different regions of the optical spectrum. In addition, P3HT nanofibers possess an ability to be aligned by an external electric field, while being dispersed in a liquid. In this manuscript we show that such collective ordering of nanofibers, similar to liquid crystal material, significantly changes the properties of transmitted light. With a specially fabricated opto-fluidic component, we monitored the phase and transmission modulation of light propagating through the solution of P3HT nanofibers, being placed in the electric field with strength up to 0.1 V/μm. This report describes a technique for light modulation, which can be implemented in optical fiber-based devices or on-chip integrated components.

References and links

1. R. M. Hyman, A. Lorenz, S. M. Morris, and T. D. Wilkinson, "Polarization-independent phase modulation using a blue-phase liquid crystal over silicon device," Appl. Opt. **53**(29), 6925–6929 (2014).
2. F. Peng, Y. H. Lee, Z. Luo, and S. T. Wu, "Low voltage blue phase liquid crystal for spatial light modulators," Opt. Lett. **40**(21), 5097–5100 (2015).
3. J. Yan, Y. Xing, Z. Guo, and Q. Li, "Low voltage and high resolution phase modulator based on blue phase liquid crystals with external compact optical system," Opt. Express **23**(12), 15256–15264 (2015).
4. Z. Zalevsky, "Integrated micro-and nanophotonic dynamic devices: A review," J. Nanophotonics **1**(1), 012504 (2007).
5. V. G. Chigrinov, "Liquid crystal applications in photonics," Proc. SPIE **7232**, 72320P (2009).
6. H. Ren, Y. H. Lin, Y. H. Fan, and S. T. Wu, "Polarization-independent and fast-response phase modulators using double-layered liquid crystal gels," Appl. Phys. Lett. **86**, 141110 (2006).
7. Y. H. Lin, H. Ren, Y. H. Wu, Y. Zhao, J. Fang, Z. Ge, and S. T. Wu, "Polarization-independent liquid crystal phase modulator using a thin polymer-separated double-layered structure," Opt. Express **13**(22), 8746–8752 (2005).
8. T. J. Wang, C. K. Chaung, W. J. Li, T. J. Chen, and B. Y. Chen, "Electrically tunable liquid-crystal-core optical channel waveguide," J. Lightwave Technol. **31**(22), 3570–3574 (2013).
9. A. Fratalocchi, R. Asquini, and G. Assanto, "Integrated electro-optic switch in liquid crystals," Opt. Express **13**(1), 32–37 (2005).

10. M. R. Shenoy, M. Sharma, and A. Sinha, "An electrically controlled nematic liquid crystal core waveguide with a low switching threshold," J. Lightwave Technol. **33**(10), 1948–1953 (2015).
11. L. De Sio, M. Romito, M. Giocondo, A. E. Vasdekis, A. De Luca, and C. Umeton, "Electro-switchable polydimethylsiloxane-based optofluidics," Lab Chip **12**(19), 3760–3765 (2012).
12. A. D. Alessandro, L. Martini, L. Civita, R. Beccherelli, and R. Asquini, "Liquid crystal waveguide technologies for a new generation of low-power photonic integrated circuits," Proc. SPIE **9384**, 93840L (2015).
13. X. Guo, X. Yang, S. Li, Z. Liu, M. Hu, B. Qu, and L. Yuan, "An integrated nematic liquid crystal in-fiber modulator derivates from capillary optical fiber," Opt. Commun. **367**, 249–253 (2016).
14. H. Yu, D. Y. Kim, K. J. Lee, and J. H. Oh, "Fabrication of one-dimensional organic nanomaterials and their optoelectronic applications," J. Nanosci. Nanotechnol. **14**(2), 1282–1302 (2014).
15. L. Sardone, V. Palermo, E. Devaux, D. Credgington, M. D. Loos, G. Marletta, F. Cacialli, J. V. Esch, and P. Samorì, "Electric-field-assisted alignment of supramolecular fibers," Adv. Mater. **18**(10), 1276–1280 (2006).
16. S. Movnihan, P. Lovera, D. O'Carroll, D. Iacopino, and G. Redmond, "Alignment and dynamic manipulation of conjugated polymer nanowires in nematic liquid crystal hosts," Adv. Mater. **20**(13), 2497–2502 (2008).
17. D. Iacopino and G. Redmond, "Synthesis, optical properties and alignment of poly(9,9-dioctylfuorene) nanofibers," Nanotechnology **25**(43), 435607 (2014).
18. G. S. Lobov, Y. Zhao, A. Marinins, M. Yan, J. Li, M. S. Toprak, A. Sugunan, L. Thylen, L. Wosinski, M. Östling, and S. Popov, "Electric field induced optical anisotropy of P3HT nanofibers in a liquid solution," Opt. Mater. Express **5**(11), 2642 (2015).
19. G. S. Lobov, Y. Zhao, A. Marinins, M. Yan, J. Li, M.S. Toprak, A. Sugunan, L. Thylen, L. Wosinski, M. Östling, and S. Popov, "Dynamic manipulation of optical anisotropy of suspended poly-3-hexylthiophene nanofibers," Adv. Opt. Mater. **4**(10), 1651–1656 (2016).
20. Y. Zhao, A. Sugunan, D. B. Rihtnesberg, Q. Wang, M. S. Toprak, and M. Muhammed, "Size-tuneable synthesis of photoconducting poly-(3-hexylthiophene) nanofibres and nanocomposites," Phys. Status Solidi., C Curr. Top. Solid State Phys. **9**(7), 1546 (2012).
21. S. Nemoto, "Measurement of the refractive index of liquid using laser beam displacement," Appl. Opt. **31**(31), 6690–6694 (1992).
22. W. Ahmed, E. S. Kooij, A. van Silfhout, and B. Poelsema, "Quantitative analysis of gold nanorod alignment after electric field-assisted deposition," Nano Lett. **9**(11), 3786–3794 (2009).
23. J. J. Boote and S. D. Evans, "Dielectrophoretic manipulation and electrical characterization of gold nanowires," Nanotechnology **16**(9), 1500–1505 (2005).
24. E. Weber, F. Keplinger, and M. J. Vellekoop, "On-chip light modulation applying optofluidic principles," IEEE Sens. J. **13**(12), 4773–4779 (2013).
25. G. S. Lobov, Y. Zhao, A. Marinins, M. Yan, J. Li, M. S. Toprak, A. Sugunan, L. Thylen, L. Wosinski, M. Östling, and S. Popov, "Size Impact of Ordered P3HT Nanofibers on Optical Anisotropy," Macromol. Chem. Phys. **217**(9), 1089–1095 (2016).

1. Introduction

Modern demands for photonic devices impose requirements on energy consumption efficiency, performance, low cost manufacturing and applicability. This often leads to technological compromises and to the search for new advanced materials and techniques. For example, electro-optical crystals, widely employed in fabrication of optical modulators, are fast but not silicon compatible, which is a great disadvantage. Photonic devices based on electro-optical polymers can be silicon compatible, but the issues related to the performance stability issues are still unresolved. Liquid crystals (LCs) possess a strong electro-optic response due to high optical anisotropy and ability to be oriented by external electric field. Despite the comparatively slow switching speed, LCs are used in ubiquitous applications [1–5]. However, LCs are not widely spread in integrated photonics, which is a cornerstone for modern advanced technologies. Since the orientation of LCs is strongly dependent on the topology of the sidewall surface, LCs form randomly oriented scattering domains and introduce losses if the walls of the optical waveguide are not specifically treated [6]. Combining LCs with a polymer host matrix helps to minimize the domain size, but drastically increases the operating voltage [7]. Therefore, the implementation of LCs in waveguide-integrated devices inevitably limits their applicability [8–13].

One-dimensional (1D) organic nanostructures can be considered as another type of material with unique anisotropic properties, which can outperform properties of well-known materials and be enhanced by introducing a structural alignment at a macroscale [14,15]. Similarly to LCs, for implementation of organic 1D nanostructures in active electro-optical applications, it is necessary to be able to dynamically and reversibly control their spatial

alignment. Until now, the commonly used approach was based on introducing desired nanostructures into a liquid crystal matrix, wherein the alignment of the dopants was imposed by ordering of the matrix [16]. However, this method inherits all the common disadvantages of using LCs.

In this article we demonstrate that organic 1D nanostructures can be used as an active material for light modulation. We used P3HT nanofibers, which are polymeric p-type semiconducting crystals formed by the π-π stacking and van der Waals interactions [17]. Due to internal ordering of P3HT nanofibers, they exhibit anisotropic optical properties, which include polarization dependent absorption at wavelengths 500 - 600 nm and optical birefringence at 600 – 1700 nm [18,19]. However, the key property, which allows the electro-optical interaction, is the ability of P3HT nanofibers to be aligned by external alternate electric field. An electrostatic field acting on nanofibers, dispersed in solution, causes redistribution of positive charges along the nanofiber axis and forces nanofibers to migrate towards the negative polarity electrode. Nevertheless, if the polarity of electric field periodically changes with some frequency, nanofibers only attain a certain degree of alignment, which can be dynamically switched by changing the direction of electric field. Further we demonstrate that this method works for controlling the alignment of P3HT nanofibers inside a hollow core of a micro-structured optical fiber. Depending on the wavelength and polarization of the probe beam, we achieved transmission and direct birefringence modulation. Unlike LCs-based techniques, our method does not require treatment of the inner waveguide surface. P3HT nanofibers do not form scattering domains and do not change the polarization of light in the off-state. The described technique can also be suitable for studying of any dispersed electro-optical material.

2. Experimental method and simulations

At first, P3HT nanofibers with lengths of 1-1.5 μm were fabricated by the mixed solvent method [20]. Nanofibers produced by this method come in the form of positively charged high aspect ratio macromolecules, homogeneously dispersed in anisole. We aimed to measure how the orientation of P3HT nanofibers in solution changes the properties of transmitted light. Due to birefringence property of P3HT nanofibers, the transmitted light with polarization perpendicular to the nanofiber's axis (π-π stacking axis) travels faster than the one with the parallel polarization. Therefore, the propagation of linearly polarized light through dispersed P3HT nanofibers can be described by a model of a plane wave travelling in a uniaxial media (Fig. 1). In such a case, by aligning the nanofibers vertically (90°) (Fig. 1(b)) or horizontally (0°) (Fig. 1(c)), the transmitted light, linearly polarized to 45° with respect to the x- and y- axis (Fig. 1(a)), becomes elliptically polarized. The orientation of the output elliptical polarization depends on the sign of the mutual phase shift $\pm \Delta\varphi$. Since P3HT nanofibers have maximum value of birefringence at wavelengths 600-650 nm [19], for experiments with the phase shift modulation we used a 632 nm light source polarized to 45° with respect to the horizontal and vertical nanofibers alignment.

The transmission modulation was achieved using dichroic properties of P3HT nanofibers. For the spectral range of 500-600 nm, the polarization of light perpendicular to the nanofiber's axis is absorbed stronger than the parallel one. Therefore, when the alignment of nanofibers coincides with the input polarization of light, it corresponds to the minimum of absorption, and oppositely, to the maximum of absorption when the polarization and the alignment are crossed. In transmission modulation experiments we used a 532 nm light vertically (90°) polarized.
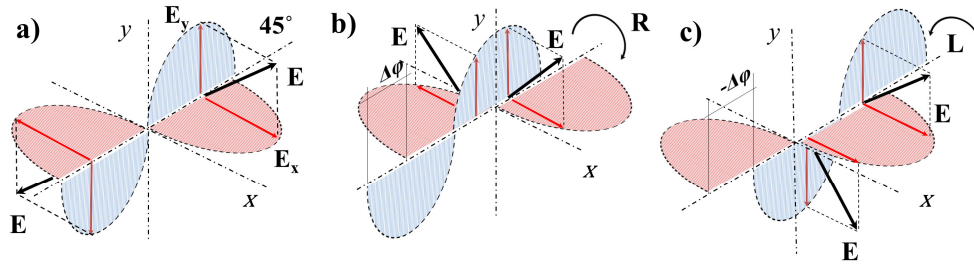
Fig. 1. The conversion of linear 45° polarization (a) into right elliptical, (b) and left elliptical (c) state, while light propagates through a uniaxial media.

The key element of the measurement setup was the opto-fluidic component with a built-in 20 mm long capillary (Fig. 2), which acted as a chamber for the liquid and optical waveguide. The solution with P3HT nanofibers was introduced into the capillary by a pressure pump through a multimode fiber with two side-holes. The light was coupled in and out of the component by a pair of microscope objectives and two multimode optical fibers, connected to the input and output. The poling electrodes were formed by placing four copper wires of Ø50 µm along the capillary. Diametrically opposite wires formed two poling electrode pairs and were connected to the voltage supply with interleaving, creating an electric field inside the capillary either in the horizontal (0°) or vertical (90°) plane. Such quadrupole configuration allowed aligning the nanofibers by 0° or 90°. The distance between paired electrodes was 600 µm. The opto-fluidic component, together with the poling electrodes, formed the active component of the setup.
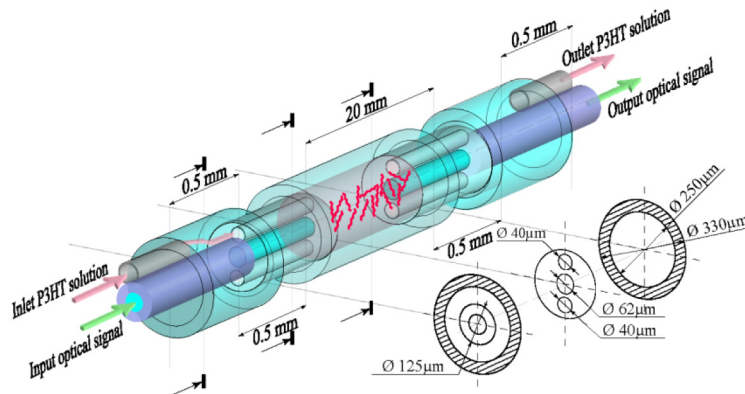

Fig. 2. The layout of the opto-fluidic part of the active component. The design is based on a micro-structured optical fiber with an optical core and 2 holes along its cladding, which is inserted into the capillary (Ø330/250 µm) from both ends. The solution of P3HT nanofibers is injected through the inlet pipe, flows through the cladding holes, fills the capillary and flows out from the outlet. The light can be simultaneously introduced through the multimode optical fiber, which is spliced to the core of the 2 holes fiber. The same liquid-light manifold configuration is built at the output side, where liquid and light become separated. In this case, the capillary acts as a light-liquid interaction chamber.

The overall measurement setup included two monochromatic light sources: HeNe laser (632 nm) and LED (532 nm), the active component and the read-out equipment, consisting of a polarimeter and a powermeter (Fig. 3). After the capillary was filled, the inlets and outlets were sealed to prevent the liquid from passive flow and evaporation. The refractive index of the capillary and the anisole solvent at 589 nm were 1.46 and 1.516, respectively. The refractive index of the P3HT solution at 632 nm was measured by the laser beam displacement technique and was 1.60 ± 0.03 [21]. The degree of polarization (DOP) of

transmitted light after filling the opto-fluidic component was around 86%, which indicates that the initial polarization was sufficiently well maintained. The offset values of the phase shift measured before the experiments were used as a zero level.
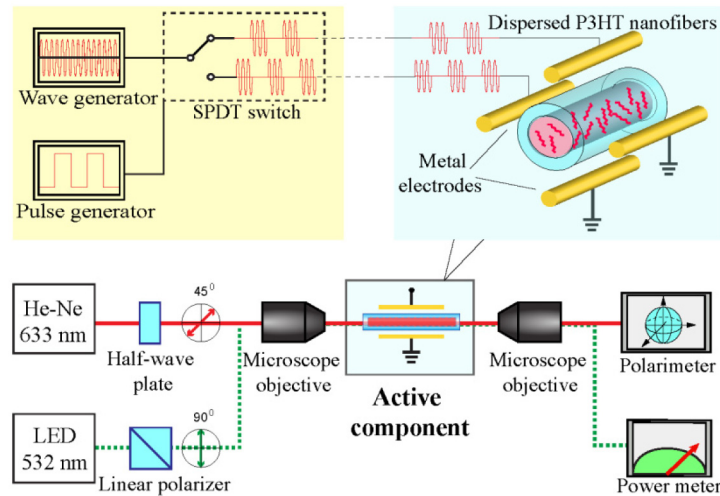

Fig. 3. The schematic of the measurement setup.

Due to the positive charge of the P3HT nanofibers [18], the poling process required the pair of electrodes to be biased to an alternating voltage supply. This was done by amplifying a bipolar sine signal from a wave generator with variable amplitude and frequency. For a sequential switching between the electrode pairs we designed an electric circuit with a single pole double throw (SPDT) switch. The SPDT switch was controlled by square wave pulses of predefined rate and duty cycle. In this way, when the control pulse was received by the circuitry, the electric potential was switched to the top electrode, while all the others were grounded. In the absence of the control pulse, the electric potential was switched to the top, right and bottom electrodes, while the left electrode was grounded. Such circuitry design did not provide a perfectly uniform electric field distribution inside the capillary, but allowed avoiding unwanted floating potentials.

In order to estimate the electric field distribution inside the capillary, we used numerical simulations (Fig. 4). The main result of the simulations was the relation between the poling voltage 'V' and the amplitude value of electric field, which serves as a figure of merit for evaluation of the electro-optical response. As the alignment of nanofibers depends on the poling voltage, and the capacitance between the poling electrodes was considered to be negligible, it was sufficient to account the problem in the electrostatic domain. With such an assumption, the modeled electrode potential corresponds to the amplitude value of the poling voltage "V". The positive charge carried by nanofibers and possible charging of the outer dielectric surface of the capillary were not taken into account. The dielectric constant of the liquid inside the capillary was 4.33, corresponding to the dielectric constant of anisole. The colors in Fig. 4(a) and 4(b) represent the magnitude of the normalized electric field. In both cases, the electric field lines are distributed uniformly only in the center of the capillary. Figure 4(d) and 4(e) provide a description to Fig. 4(a) and show the EX and EY components along the orthogonal axes (marked as X and Y) and EY at three points (marked in Fig. 4(c) as '1','2','3') versus applied poling voltage. According to the plotted data, the gradient of electric field in proximity to the capillary inner walls may cause a slow dielectrophoretic (DEP) transition of the nanofibers [22,23], In such a case, the nanofibers in the center of the capillary should stay stationary and contribute mostly to the modulation, while nanofibers at the periphery may drift towards the electrodes and locate in the proximity to the capillary

inner walls. Values of the EY and EX components for powered vertical pair of electrodes (Fig. 4(a)), averaged over the entire inner capillary cross section, are plotted in Fig. 4(f). The EY component is approximately 5 times larger than the EX, which explains why the nanofibers are dominantly aligned along the Y-axis.
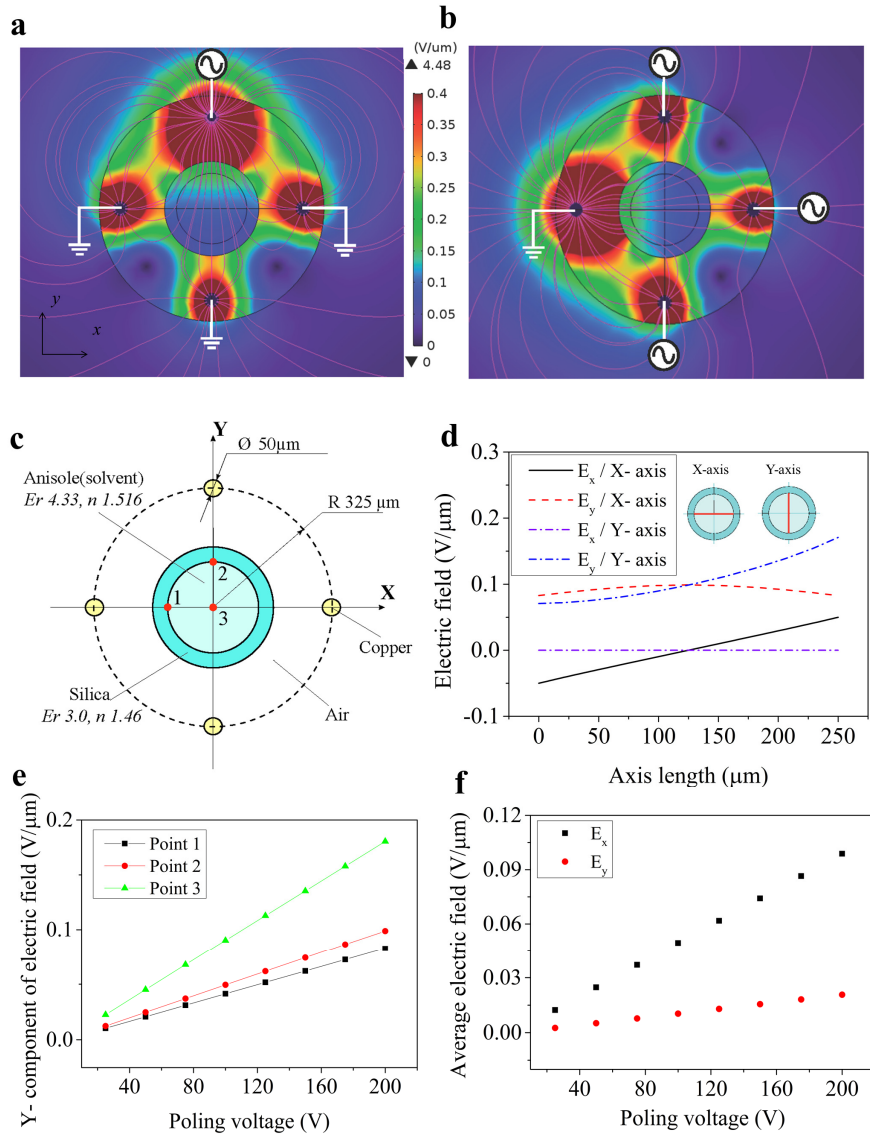

Fig. 4. The simulation results. Configuration of electric field for (a) vertically and (b) horizontally powered electrodes; (c) description of the computational domain; (d) E_X and E_Y electric field components along the X and Y axes for vertically powered electrodes; (e) E_Y electric field component for vertically powered electrodes; (f) electric field averaged over the capillary cross section.

3. Measurement results and discussions

The measurement results are presented in Fig. 5, where the right and left elliptical polarizations are represented in terms of positive and negative increments of mutual phase shift, respectively (Fig. 5(a)). The initial zero value of phase shift corresponds to the moment

when the poling voltage was not switched on. Interesting to note, when the voltage was switched off, the output polarization returned to linear state, indicating that nanofibers relaxed to a disordered configuration. We measured the switching time as an average value of time required to switch from the negative increment to the positive one ('switching up') and vice versa ('switching down'). The amplitude of phase shift was measured as the difference between the absolute maxima of both increments. The amplitude of phase shift equal to $\pi/2$ was achieved at 120 V (Fig. 5(b)), which corresponds to electric field in the capillary center of 0.11 V/μm (Fig. 4(c), point '3'). At average electric field of 0.1 V/μm the optical phase shift and switching time were $5/6\pi$ and 26 ms, respectively.
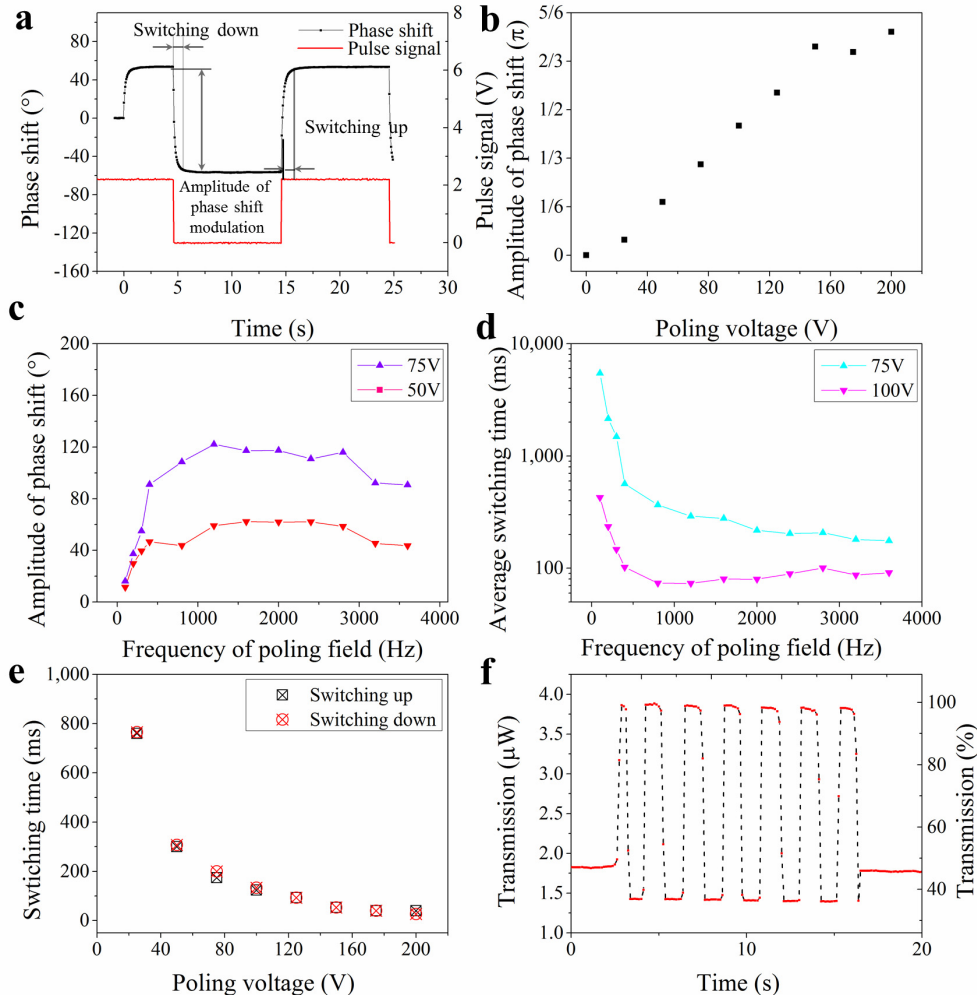

Fig. 5. Results of birefringence and transmission modulation measurements: (a) a plot showing the phase shift of transmitted light with respect to the control signal; (b) amplitude of phase shift versus poling voltage; (c) amplitude of phase shift versus frequency of poling voltage; (d) average switching time versus frequency of poling voltage; (e) switching time versus poling voltage measured at poling voltage frequency of 2 kHz; and (f) transmission modulation plot measured at poling voltage of 215 V and poling voltage frequency of 2 kHz.

The phase shift and switching time increased with the frequency of poling voltage, and reached the saturation at approximately 800 Hz (Fig. 5(c) and 5(d)). This can be attributed to charging of the capillary outer surface. In such a way, accumulated charges form a screening layer, which may effectively decrease the poling electric field. Presumably, due to a limited

rate of charging, this process becomes negligible when the frequency of electric field reaches a certain threshold. The relation between the switching time and the poling voltage is shown in Fig. 5(e) (measured in separate experiments).

The results of transmission modulation are shown in Fig. 5(f). At poling voltage of 213 V and frequency 2000 Hz the modulation depth reached 2.71, which is a ratio between the maximum and minimum transmission levels. Due to high absorption of P3HT nanofibers at 532 nm, we diluted the solution 20 times for the transmission modulation measurements.

In order to give an indication of P3HT nanofibers optical stability and robustness, we conducted a stress test using a 20 times diluted concentration. We set the frequency of controlling pulses to 8 Hz, which corresponds to 16 switching cycles per second, and monitored the amplitude of phase shift modulation over a period of time. The experiment was stopped when the amplitude of phase shift dropped by 5%, after 1506 seconds of modulation or 2.41×10^4 switching. Figure 6 shows the Poincare sphere with a trace of polarization states observed at the beginning and at the end of the experiment. The reason for the phase shift drop of 5% can be explained by a slow transition of nanofibers towards the capillary walls due to dielectrophoresis. As it can be seen in Fig. 6, the dotted trace forms a straight line, which indicates that the motion of nanofibers was stable and repeatable during the entire measurement process. More tests need to be done to study long-term stability and influence of different parameters on the nanofibers behavior.
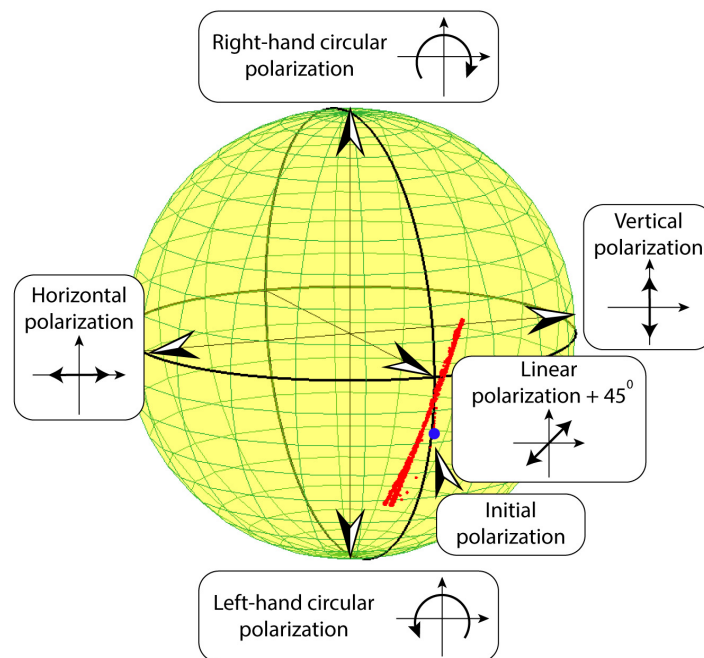

Fig. 6. Poincare sphere with polarization states traced during continuous modulation of phase shift at poling voltage of 213 V, poling voltage frequency of 2 kHz and switching rate of 16 Hz; the blue point represents the initial state of polarization before the start of the measurement.

Using scanning electron microscope, we experimentally defined that 1 μl of undiluted solution contains approximately $5.6 \cdot 10^8$ nanofibers. This density corresponds to spacing between individual nanofibers of several micrometers. Hence, assuming that nanofibers are evenly distributed in the solution, it can be considered that they have enough space to rotate freely without clogging and interfering with each other. However, it is possible to fabricate

P3HT nanofibers in solution with the density of 113×10^8 units/μl and with no aggregation effects.

It is important to address the issues related to self-relaxation mechanism. When the nanofibers are aligned under an electric field, the positive charges on the nanofibers accumulate at their tips directed towards the negative polarity electrode. In this case, the electrostatic repulsive forces between the positive charges are balanced by the stronger poling forces. When the poling field is switched off, the nanofibers relax to a disordered state under repulsive forces. An important conclusion can be drawn: the increase of nanofibers concentration leads to a more tight packing, stronger repulsive forces and, therefore, shorter relaxation time. On the other hand, a significant decrease of the concentration may totally cancel the relaxation mechanism, forming a memory effect. An adjustable relaxation time may have a significant value for the development of planar on-chip devices that can employ only one pair of electrodes. Modern opto-fluidic principles and silicon-based technology can be used to construct an on-chip single mode optical waveguide with poling electrodes integrated onto its sidewalls and introduced P3HT nanofibers solution acting as a core material [24]. In such a case, assuming that the distance between the electrodes is around 10 μm, the poling fields of 0.1 V/μm may be achieved at voltage of approximately 1 V. According to the previous results, the degree of alignment increases linearly with the magnitude of electric field up to the value of 0.8 V/μm [25]. Therefore, using the same density of P3HT nanofibers as in our experiments (5.6×10^8 units/μl), the amplitude of phase shift equal to π (using a 633 nm probe beam) may be achieved with a waveguide length of 3.3 mm and a poling voltage of 8 V. The increase of P3HT nanofibers density can potentially enhance the performance even more and allow using a shorter waveguide.

The birefringence of aligned P3HT nanofibers can be calculated using Eq. (1), where θ - is the amplitude of phase shift, λ - optical wavelength, d– length of the capillary.

$$\Delta n = \frac{\theta / 2 \cdot \lambda}{2\pi d} \tag{1}$$

For the phase shift amplitude of $5/6\pi$, observed at 633 nm for average poling electric field of 0.1 V/μm, the birefringence is 6.5×10^{-6}. This value can be further enhanced by increasing the poling electric field and by using solution with a higher concentration of P3HT nanofibers.

According to the measurement and simulation results, the acquired phase shift was linearly proportional to the poling voltage for the larger part of the curve (Fig. 5(b)), which, in turn, was in linear relation with the amplitude of poling field strength (Fig. 4(f)). Such behavior is surprising, as the linear relation between the birefringence and the electric field is characteristic for the second order electro-optical effects, such as the Pockels effect, which are not observed in centrosymmetric systems. This should be studied deeper in further studies.

4. Conclusions

In summary, we demonstrated a new approach for modulation of light, based on controllable rotation of dispersed P3HT nanofibers in an opto-fluidic component. Rotation of nanofibers was implemented by applying external alternating electric field and was dynamically controlled by using a quadrupole configuration of electrodes. The anisotropic properties of P3HT nanofibers allow transmission modulation for optical wavelengths below 600 nm and direct birefringence modulation for spectral range 600-1500 nm.

The modulation efficiency can be easily enhanced by using a longer capillary. The response time and the degree of alignment can be further improved by increasing the poling field and optimizing the density of nanofibers.

The described technique implies many new applications, from polarization maintaining devices to adaptive optical components and modulators. The self-relaxation mechanism opens up opportunities for planar devices, where only one pair of electrodes can be used. With further development, it can be potentially realized in an integrated chip device, using well known microfluidic techniques.

5. Fabrication of P3HT nanofibers

P3HT nanofibers were fabricated via the mixed solution method. 10 mg of P3HT (regioregularity > 95%, Luminescence Technology Corporation Taiwan, China) was mixed with 5 ml of anisole (anhydrous, 99.7%, Sigma Aldrich) and was sonicated for 10 minutes. Further, after adding 5 ml of chloroform (99%, VWR) the solution was sonicated for 10 minutes and placed in a dark box for 72 hours with continuous nitrogen flow. At the final stage the solution was diluted with anisole according to 1:20 ratio.